ResearchGate

See discussions, stats, and author profiles for this publication at: https://www.researchgate.net/publication/231649062

Adsorption of O−2, H−2, CO, NH3, and NO2 on ZnO nanotube: A density functional theory study

ARTICLE *in* THE JOURNAL OF PHYSICAL CHEMISTRY C · MARCH 2008

Impact Factor: 4.77 · DOI: 10.1021/jp711105d

CITATIONS
110

READS
227

3 AUTHORS, INCLUDING:

Wei An
Shanghai University of Engineering Science
47 PUBLICATIONS **1,094** CITATIONS
SEE PROFILE

Xiaojun Wu
University of Science and Technology of China
114 PUBLICATIONS **2,337** CITATIONS
SEE PROFILE

Available from: Wei An
Retrieved on: 25 January 2016

Adsorption of O_2, H_2, CO, NH_3, and NO_2 on ZnO Nanotube: A Density Functional Theory Study

Wei An, Xiaojun Wu, and X. C. Zeng*

Department of Chemistry and Nebraska Center for Materials and Nanoscience, University of Nebraska-Lincoln, Lincoln, Nebraska 68588

Received: November 22, 2007; In Final Form: January 5, 2008

Using density functional theory (DFT), we have investigated the structural and electronic properties of a prototype ZnO (6,0) zigzag single-walled nanotube (SWNT) with and without oxygen vacancy (V_O), as well as its potential application as a sensor for gas molecules O_2, H_2, CO, NH_3, and NO_2. The DFT calculation shows that the defect-free ZnO (6,0) SWNT is semiconducting with a direct band gap larger than that of bulk ZnO. By introducing the V_O defects, localized impurity states are induced above the valence band maximum while the Fermi level is lifted. As such, the defect-containing ZnO (6,0) SWNT becomes an *n*-type semiconductor. On the sidewall of a defect-free ZnO (6,0) SWNT, O_2 and H_2 molecules are physisorbed while CO, NH_3, and NO_2 are molecularly chemisorbed. With the V_O defects, the binding interaction between gas molecules and the ZnO nanotube becomes stronger. The electron-donor molecules (CO and NH_3) tend to enhance the concentration of major carriers (electrons), whereas the electron-acceptor molecules (O_2 and NO_2) tend to reduce the concentration. Moreover, we find that O_2 and NO_2 can dissociate at the V_O sites through filling the V_O with one atomic O originated from the adsorbates. The dissociation of O_2 is exothermic and barrierless while the dissociation of NO_2 is also exothermic but entails a small activation barrier (0.49 eV).

1. Introduction

Detection of gas molecules relevant to chemical and biochemical processes is of critical importance in industrial, environmental, and medical monitoring.[1,2] In practice, solid-state gas sensors are commonly utilized for the monitoring task. Semiconducting metal oxides have been considered as best materials for making gas sensors because of advantages such as low cost, small dimensions, and great compatibility with microelectromechanical processing. The conventional sensing mechanism is such that upon exposure to the target gas molecules charge transfer between the adsorbed gas species and the surface of semiconducting metal oxides occurs. This charge transfer will either increase or decrease the concentration (or mobility) of the major carriers in the metal oxides, depending on the semiconductor type, thereby increasing or decreasing the electrical conductance of the sensor under operating conditions.

Bulk zinc oxide (ZnO) is known as an ionic semiconductor with a wide and direct band gap (3.4 eV).[2b] Among other applications, ZnO has been studied extensively for its potential use as a gas sensor[1−9] or even as a biosensor owing to the excellent biocompatibility of ZnO surface. However, it has been found that polycrystalline ZnO, when integrated into film[2−5] or ceramics,[6−9] shows only limited sensitivity for gas-sensor application, largely because of the low surface-to-volume ratio with which only a small fraction of gas molecules adsorbed within the grain boundaries can affect electrical conduction. Additionally, high sensitivity of the thin-film gas sensors can be only realized at elevated temperatures. Alternatively, one-dimensional (1D) ZnO nanotubes (NTs), nanorods (NRs), or nanowires (NWs) have shown much higher sensitivity than polycrystalline ZnO at room temperature because of their higher surface-to-volume ratio and stronger dependence of electrical conductance on the amount of adsorbates.[10−14] Moreover, the gas sensors fabricated with the 1D ZnO nanostructures have shown some advantages over conventional materials in terms of low power consumption, light weight, fast response, and easy recovery capability.

Many experimental studies have been devoted to investigating the characteristics of various gas molecules on ZnO NTs or NRs, including O_2,[10,11] H_2,[12−14] O_3,[12b] LPG (C_3−C_4 hydrocarbon),[13] CO,[14] NH_3,[14−16] NO_2,[15] H_2S,[17,18] ethanol,[17,19] and glucose.[20] However, to our knowledge, no theoretical studies have been reported to investigate microscopic interactions between target gas molecules and 1D ZnO NTs. Detailed molecular understanding of how adsorbates can modify electronic structures of ZnO NTs is still lacking. In this article, we present a density functional theory (DFT) study of the adsorption of various gas molecules (O_2, H_2, CO, NH_3, and NO_2) on a prototype ZnO NT without or with oxygen vacancies. Particular attention is paid to understanding the modification of electronic structures of ZnO NTs by the gas-molecule adsorbates.

2. Models and Methods

ZnO NTs and NRs or NWs have been synthesized in the laboratory.[21−27] One form of ZnO NTs has been characterized experimentally as a hexagonal cylinder growing in the [0001] direction (or the *c* axis) of the hexagonal ZnO bulk crystal.[24,25] Following the nomenclature of carbon nanotube, ZnO (*n*,*m*) refers to the chiral vector to locate the position on a ZnO sheet whose repeating unit is a hexagonal $(ZnO)_3$ lattice. In this study, we chose a prototype single-walled zigzag ZnO (6,0) nanotube as the model adsorbent. Because the occurrence of oxygen

* Corresponding author. E-mail: xczeng@phase2.unl.edu.

10.1021/jp711105d CCC: $40.75 © 2008 American Chemical Society
Published on Web 03/25/2008

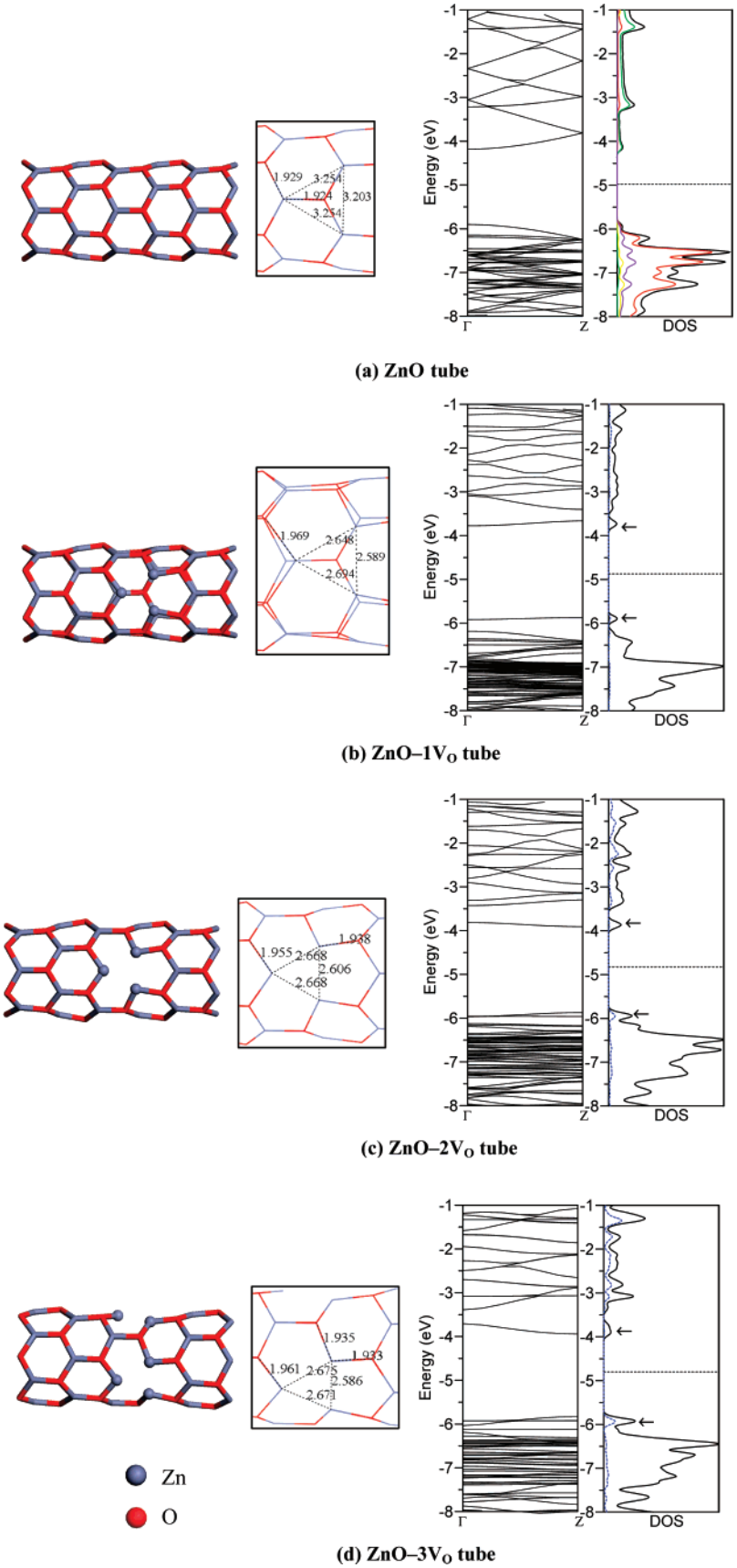

Figure 1. Optimized geometric structures (left panel) and electronic band structure and the total density of states (right panels) for pristine ZnO (6,0) SWNT with (a) no defect, (b) one, (c) two, and (d) three oxygen vacancies ($1V_O$, $2V_O$, and $3V_O$). The middle insets show $Zn(V_O)-Zn(V_O)$ distances near the V_O sites. The dotted line denotes the Fermi level E_F, which is −4.98, −4.87, −4.83, and −4.80 eV for ZnO (6,0), ZnO (6,0)−$1V_O$, ZnO (6,0)−$2V_O$, and ZnO (6,0)−$3V_O$ SWNT, respectively. Red, green, yellow, and purple solid lines in (a) represent the partial density of states (DOS) projected on p orbitals of O atoms and s, p, and d orbitals of Zn atoms, respectively. The blue dashed lines in (b)−(d) illustrate the partial DOS projected on Zn atoms at the V_O site. The arrows mark the impurity states due to the Vo defects.

TABLE 1: Adsorption Energy (E_{ad}),[a] Partial Charge Transfer (δq),[b] and Binding Distance (d)[c] for Various Adsorbates on the ZnO (6,0) SWNT with Zero, One, or Three Oxygen Vacancies (V_O)

	E_{ad} (eV)	δq (e)	d (Å)
O_2	−0.048	−0.011	2.667
H_2	−0.031	0.00	2.529
CO	−0.22	0.18	2.319
NH_3	−0.82	0.26	2.162
NO_2	−0.30	−0.22	2.245
NH_3 ($\theta = 1/6$ ML)	−0.75	0.23	2.177
NO_2 ($\theta = 1/6$ ML)	−0.22	−0.10	2.410
NH_3 ($\theta = 1/3$ ML)	−0.25	0.18	2.250
NO_2 ($\theta = 1/3$ ML)	−0.16	−0.08	2.398
O_2/V_O	−1.73	−0.79	1.926
$3O_2/3V_O$ ($\theta = 1/6$ ML)	−1.55	−0.80	1.922
NH_3/V_O	−0.91	0.25	2.190
NO_2/V_O	−0.98	−0.28	2.098

[a] For the binding of adsorbates at different coverage θ, E_{ad} is the adsorption energy per molecule. [b] Charge transfer is calculated via Mulliken charge analysis, and positive δq denotes charge transfer from adsorbate to adsorbent (ZnO NT). [c] Binding distance d is defined as the shortest distance between the adsorbate and the sidewall.

vacancies (V_O) is expected within ZnO NT at elevated temperatures, we have considered ZnO NT with different fraction of V_O defects on the sidewall to investigate the role of Vo defects on gas-molecule sensing. Five gas molecules, including O_2, H_2, CO, NH_3, and NO_2,were chosen as target molecules. For each gas-molecule species, we examined a number of adsorbate orientations as well as different adsorption sites on the sidewall of ZnO NT, for example, the top (above the Zn or O atom), bridge (above the Zn−O bond), and hollow [above the $(ZnO)_3$ hexagon] site in order to locate the lowest-energy configuration for the adsorbate/adsorbent system.

The DFT calculation was carried out using the DMol[3] package.[31] Spin-unrestricted DFT within the generalized-gradient approximation (GGA) in the Perdew−Burke−Ernzerhof (PBE) form[32] was used for the calculation. Specifically, the effective core potential (ECP) and a double numerical basis set including d polarization function (DNP) were used to obtain all of the numerical results given below. Within the ECP scheme implemented in Dmol,[3] all-electron calculation was explicitly performed for H, C, N, and O atoms. In the supercell, the zigzag ZnO (6,0) NT consists of 36 Zn and 36 O atoms. Defected ZnO NTs containing one, two, or three V_O defects per supercell ($Zn_{36}O_{35}$, $Zn_{36}O_{34}$, or $Zn_{36}O_{33}$) were studied. A $25 \times 25 \times 16.8$ Å^3 hexagonal supercell with the length of c three times that of the periodicity of ZnO (6,0) NT was set for all calculations. The minimum distance between the opposing sidewall of neighboring ZnO NTs is greater than 18.2 Å, which is sufficiently large to render interaction between the NT and its periodic images negligible. For geometry optimization and for the search of the transition state (TS), the Brillouin zone is sampled by Γ point only, which yields $0.046 \times 0.046 \times 0.060$ Å^{-1} actual spacing. For electronic structure calculations, the Brillouin zone is sampled by $1 \times 1 \times 6$ k points with 6 k points along NT axis using the Monkhorst−Pack scheme[33] in which a uniform grid of k points along the three axes in reciprocal space is produced. The real-space orbital cutoff radius was set to be 6 Å, within which atomic basis sets are confined to ensure sufficient accuracy of the DMol[3] calculations.

Adsorption energy is defined as $E_{ad} = E_{total}$[tube + adsorbate] $- E_{total}$[tube] $- E_{total}$[adsorbate], where E_{total} is the total energy of the system per supercell. Hence, negative (positive) E_{ad} denotes exothermic (endothermic) adsorption process. The minimum-energy pathway (MEP) for the NO_2 dissociation was computed using the nudged elastic band (NEB) method.[34] In essence, the NEB method starts by inserting a series of image structures between the initial and finial state of the reaction. Meanwhile, a fictitious spring force is introduced between all nearest-neighbor image structures to ensure continuity of the reaction path. By optimizing these image structures simultaneously, the MEP of the reaction can be obtained because the real force on the image structures has zero projection in the direction normal to the MEP.

3. Results and Discussion

3.1. Geometric and Electronic Structures of Pristine ZnO (6,0) SWNT. Several theoretical studies of pristine ZnO NT, NR, and NW have been reported in the literature.[28−30] A single $(ZnO)_n$ sheet is shown to be more flexible than a graphene layer.[29] In other words, it would cost less energy to roll up a planar $(ZnO)_n$ sheet to form tube-like nanostructure than rolling up a graphene layer to form CNT. Recently, Shen et al. showed that ZnO SWNT is more stable than ZnO NR or NW if the diameter is small but becomes less stable than ZnO NR or NW if the diameter is larger than that of ZnO (24,0) SWNT.[30a] Hence, the small-diameter ZnO (6,0) SWNT is expected to be more stable than ZnO NR or NW with the same diameter.

The optimized geometric structures, as well as calculated electronic band structures and the density of state (DOS) of the pristine ZnO (6,0) SWNTs with or without Vo defect, are displayed in Figure 1. The defect-free ZnO (6,0) SWNT is a symmetric cylinder with diameter $d_{O-O} = 6.768$ Å and $d_{Zn-Zn} = 6.408$ Å, whose sidewall surface is sawtooth-like because all Zn atoms are slightly protruded by O atoms. This buckling behavior on the sidewall surface is common to all zigzag polar nanotubes such as the BN (8,0) nanotube.[35] The calculated electronic band structure (Figure 1a) shows that the defect-free ZnO (6,0) SWNT is semiconducting with a direct band gap of 1.7 eV at Γ (0, 0, 0) point, larger than the calculated band gap of bulk wurtzite ZnO (∼1.2 eV at the same level of theory). A strong hybridization of Zn d and O p orbitals, which is responsible for the formation of Zn−O bonds, can be seen in the partial DOS of valence band (Figure 1a).

It is known that DFT-GGA greatly underestimates the band gap of bulk ZnO (experimental band gap is 3.4 eV at 300 K[2b]).[36,37] Previous studies have shown that DFT with a hybrid functional B3LYP can give a quantitatively more accurate (albeit empirically) band gap of the bulk ZnO.[38] We thus used the DFT-B3LYP method, implemented in CRYSTAL06 package,[39] to recalculate the band structures of bulk ZnO and ZnO (6,0) SWNT. We found that the overall features of the newly calculated band structure is nearly the same as that based on the DFT-PBE method, except the enlarged band gap, that is, 3.29 and 4.35 eV for bulk ZnO and ZnO (6,0) SWNT, respectively (see Supporting Information Figure S1), which matches the experimental band gap of bulk ZnO (3.4 eV) quite well. Because both DFT-B3LYP and DFT-PBE calculations indicate that the band gap of ZnO (6,0) SWNT is larger than that of bulk ZnO, it is expected that the qualitatively correct trend in the band structure can still be drawn from the DFT-PBE calculation. Figure 1a also shows that the valence band edge is contributed mainly by the 2p orbitals of oxygen atoms, whereas the conduction band edge is contributed largely by the 4s orbitals of zinc atoms.

Figure 1b−d shows that the presence of one, two, and three oxygen vacancies ($1V_O$, $2V_O$, and $3V_O$) per supercell in the ZnO (6,0) SWNT induces certain strain within the nanotube near the

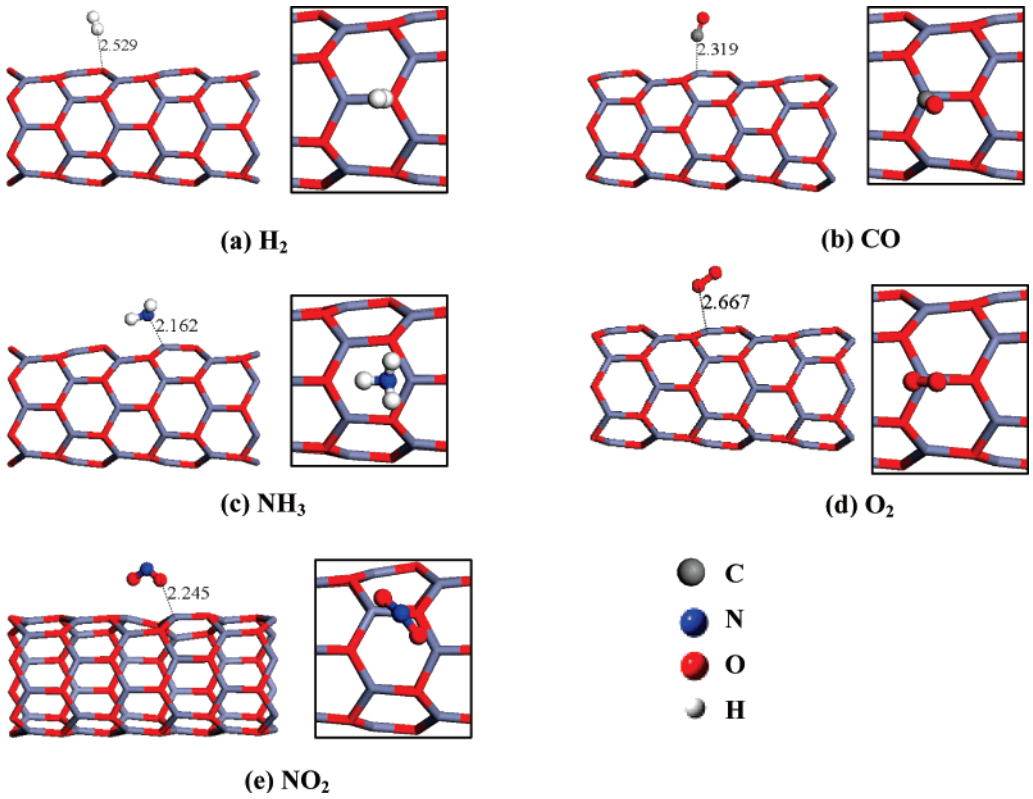

Figure 2. Most stable configuration for the adsorbate (a) H_2, (b) CO, (c) NH_3, (d) O_2, and (e) NO_2 on the defect-free ZnO (6,0) SWNT. Both side view and top view (inset) of the adsorbates are displayed with the binding distance labeled.

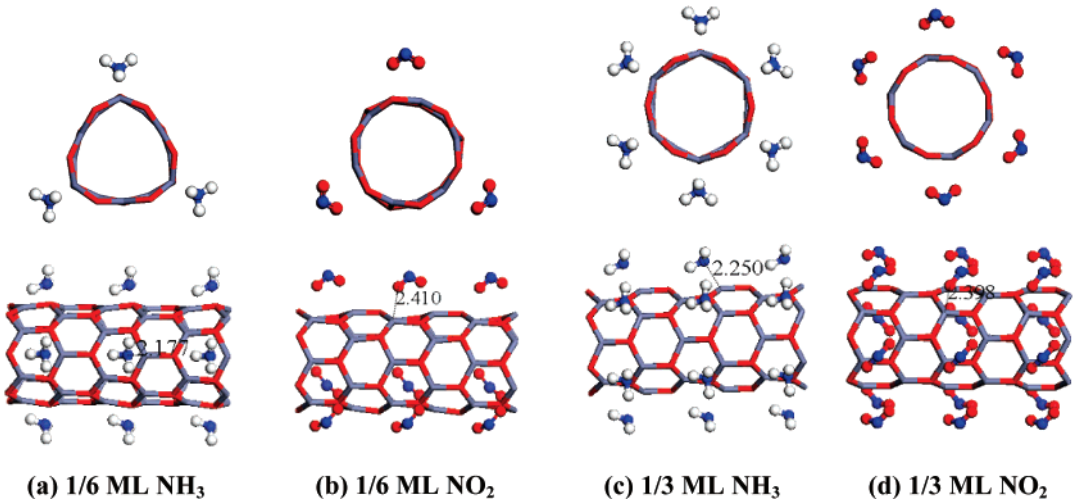

Figure 3. Most stable configuration for the adsorbate (a and c) NH_3, and (b and d) NO_2 on the defect-free ZnO (6,0) SWNT with $^1/_6$ or $^1/_3$ monolayer (ML) coverage, respectively. Both side view (lower panels) and top view (upper panels) of the ZnO SWNT are displayed with the binding distance labeled.

V_O sites, as indicated by the decrease of $Zn(V_O)-Zn(V_O)$ distances (insets in Figure 1). The ZnO (6,0) SWNTs containing $1V_O$, $2V_O$, and $3V_O$ remain to be semiconducting but some impurity states (arrows in Figure 1b−d) are introduced near the band edges. As a result, the defected ZnO (6,0) tube can be viewed as an *n*-type semiconductor. The presence of oxygen vacancies may lead to enhancement in major carrier transfer from the valence band (VB) to conduction band (CB). Moreover, a small gap opens near the CB edge. As more and more V_O sites are introduced to the ZnO (6,0) SWNT, the Fermi level is lifted slightly (at −4.98, −4.87, −4.83, and −4.80 eV with $0V_O$, $1V_O$, $2V_O$, and $3V_O$ per supercell, respectively) and the position of narrowest band gap shifts from Γ (0, 0, 0) to Z (0, 0, 0.5) point. The DOS analysis, shown in Figure 1b−d, indicates that the impurity states are mainly due to the three zinc atoms [$Zn(V_O)-Zn(V_O)-Zn(V_O)$] near the V_O site, suggesting that the electronic properties of the ZnO (6,0) SWNT can be tuned by introducing some V_O defects. The formation energy of $1V_O$, $2V_O$, and $3V_O$ defect (defined as the energy difference between the perfect tube and defective tube plus oxygen (number of vacancy) per supercell) is 6.10, 11.9, and 17.83 eV, respectively. This is an endothermic process. It should be mentioned that the positions of the V_O sites are purely hypothetic and can be viewed as the extreme configurations because only symmetric V_O sites around the tube are included (see Figure 1).

The Mulliken charge analysis shows that in the perfect ZnO (6,0) SWNT $Zn^{\delta q+}$ and $O^{\delta q-}$ bear an average Mulliken charge (δq) of 0.72 *e*, while for ZnO (6,0) SWNT containing V_O, $2V_O$,

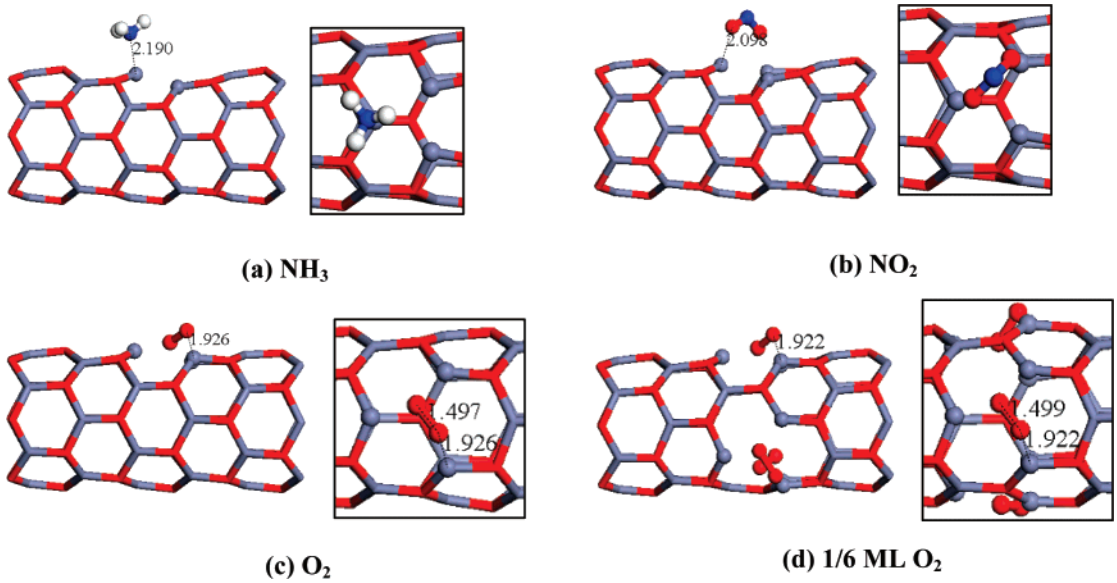

Figure 4. Most stable configuration for the adsorbate (a) NH_3, (b) NO_2, (c) O_2, and (d) O_2 with $^1/_6$ ML coverage on the ZnO (6,0)$-V_O$ SWNT. Both side view and top view (inset) of the adsorbates are displayed with the binding distance labeled.

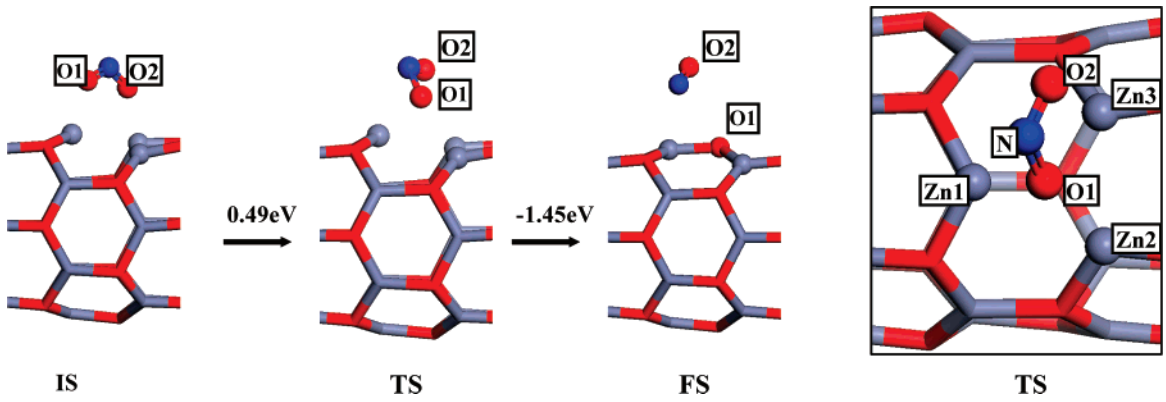

Figure 5. Side view of the local configuration of the adsorbate in the initial (IS), transition (TS), and final (FS) state along the minimum-energy pathway for NO_2 dissociation on the ZnO (6,0)$-V_O$ SWNT. The inset shows the elemental and label assignment listed in Table 2.

TABLE 2: Structural Parameters for the Initial (IS), Transition (TS), and Final (FS) States along the Minimum-Energy Pathway for NO_2 Dissociation on the ZnO (6,0)$-V_O$ SWNT

	$d_{(Zn1-O1)}$	$d_{(N-O1)}$	$d_{(N-O2)}$	∠(O1−N−O2)
IS	2.098	1.255	1.252	119.9
TS	2.020	1.427	1.211	114.6
FS	1.941	2.848	1.159	104.5

and $3V_O$ sites, the average δq on the three $Zn^{\delta q+}$ atoms near the V_O sites are reduced to ~0.47*e*. Thus, the local net Mulliken charge (δq^-) resulting from one Vo is about 0.76*e*.

3.2. Adsorption of O_2, H_2, CO, NO_2, and NH_3. O_2, H_2, and CO molecules are typical components present in feedstock for fuel cells. CO and NO_2 are common gaseous pollutants comprising the main detriment of automotive emission. NH_3 is a major chemical product in industry. As is well known, there is enriched chemistry and physics on bulk ZnO wurtzite surface.[40] Understanding the adsorption behavior of these molecules on 1D ZnO nanotubes is thus of both practical and fundamental interest. In general, adsorption behavior can be classified as physisorption, chemisorption, and molecular chemisorption. The latter is an intermediate adsorption between physisorption and chemisorption, as characterized by a small amount of charge transfer between adsorbate and adsorbent and by moderate binding energy and distance with some bond-length change at the adsorption site.

Table 1 lists the calculated adsorption energy (E_{ad}), partial charge transfer (δq), and binding distance (d) to the sidewall of ZnO (6,0) SWNT for O_2, H_2, CO, NH_3, and NO_2 in their most stable configuration (Figures 2−4). It is found that CO, NH_3, and NO_2 are molecularly chemisorbed on the defect-free ZnO (6,0) SWNT with E_{ad} of −0.22, −0.82, and −0.30 eV, respectively, whereas O_2 and H_2 are physisorbed with E_{ad} of −0.048 and −0.031 eV, respectively. Among the chemisorbed molecules, NO_2 behaves as a charge acceptor because of negative δq (−0.22*e* per molecule) whereas CO and NH_3 behave as charge donors because of positive δq (0.18*e* and 0.26*e* per molecule, respectively). The charge transfer behavior with the adsorbates is consistent with previous experimental findings in that the electronic conductance of *n*-type ZnO-NRs increases when exposed to NH_3 and CO[14−16] gases but decreases when exposed to O_2[10,11] and NO_2.[15]

Oxygen vacancies are common defects in wurtzite bulk ZnO.[2,40] As a result, the defects are more favored adsorption sites for target molecules than the perfect sites on the surface. We further calculated adsorption energies of O_2, NO_2, and NH_3 on a V_O site of the ZnO (6,0) SWNT. The optimized structures are displayed in Figure 4. As expected, the binding of the adsorbates to the V_O site is stronger than that to the perfect site (see values of E_{ad} and δq in Table 1). More interestingly, the binding character of O_2 has changed from the physisorption to

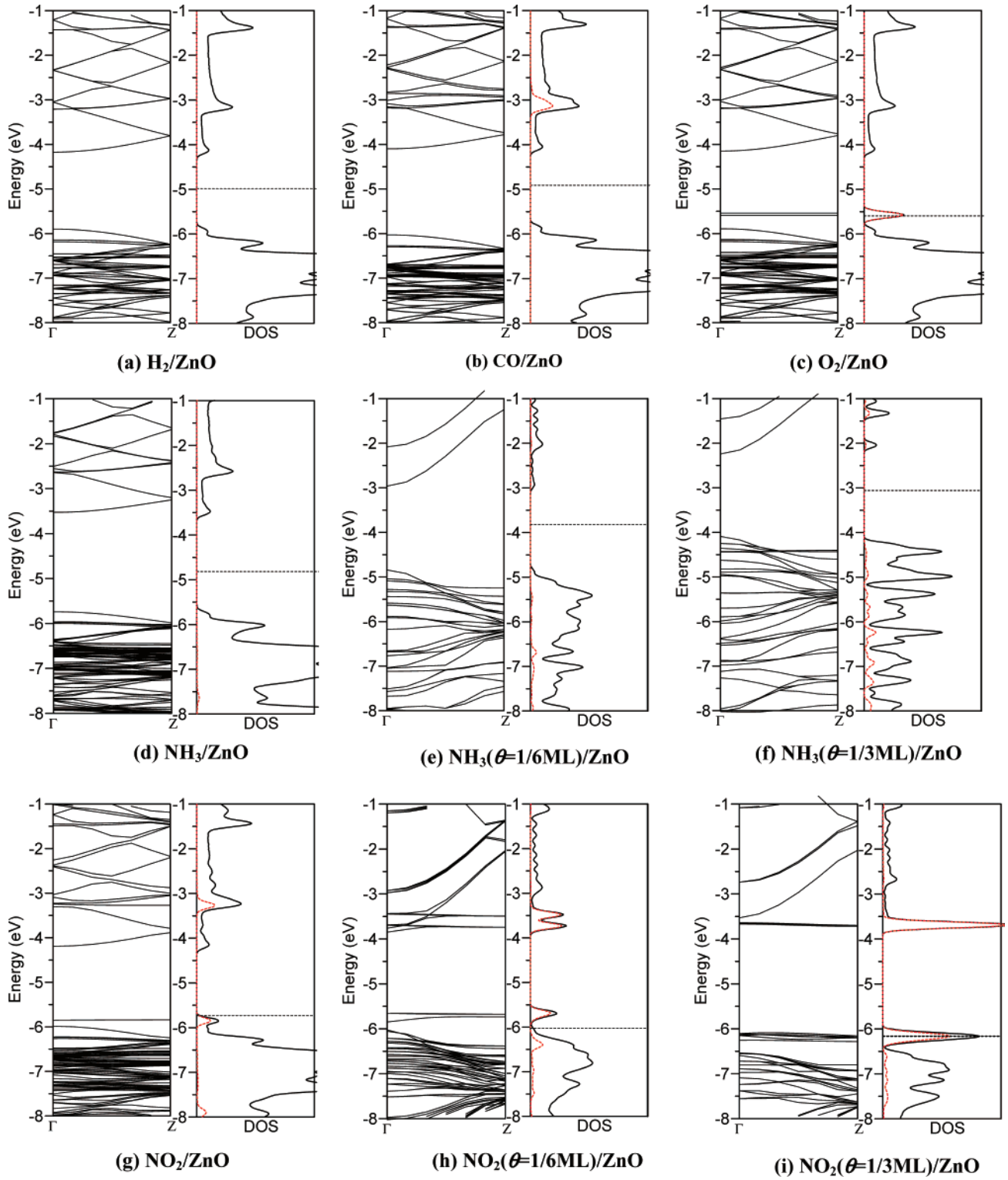

Figure 6. Electronic band structures and total DOS for various adsorbates on the ZnO (6,0) SWNT (Figures 2 and 3). Local DOS projected onto each adsorbate is plotted on the red dashed line. The black dashed lines in DOS plots (right panels) denote the Fermi level. Band structure and DOS shown in e, f, h, and i are calculated using a smaller supercell, that is, one-third of that for d and g.

dissociative chemisorption as shown by the larger E_{ad} (−1.73 eV) and δq (−0.79e), as well as the increased O···O bond length (1.497 Å). Hence, the adsorbed O_2 forms a peroxo-type structure (Figure 4c), which is quite common when O_2 is adsorbed on ionic nanostructures.[35] In fact, an O atom of the O_2 molecule can fill the V_O defect spontaneously through a barrierless dissociation process once the O_2 molecule is adsorbed on top of the V_O site. Note that this adsorption behavior of O_2 on the V_O site is apparently different from that on the V_O site of the ZnO (1010) surface,[41] for which the most favorite adsorption site is on the top of Zn(V_O)−Zn bridge bond near the V_O site. In the latter case, the adsorbed O_2 proceeds to dissociate via a redundant pathway (O−O stretch and rearrangement) to fill the V_O.

As the coverage of O_2 and V_O sites increases (Figure 4d), the binding character of O_2 on the V_O sites remains nearly unchanged with $E_{ad} = -1.55$ eV and $\delta q = -0.80e$. Our calculations appear to be consistent with a well-accepted

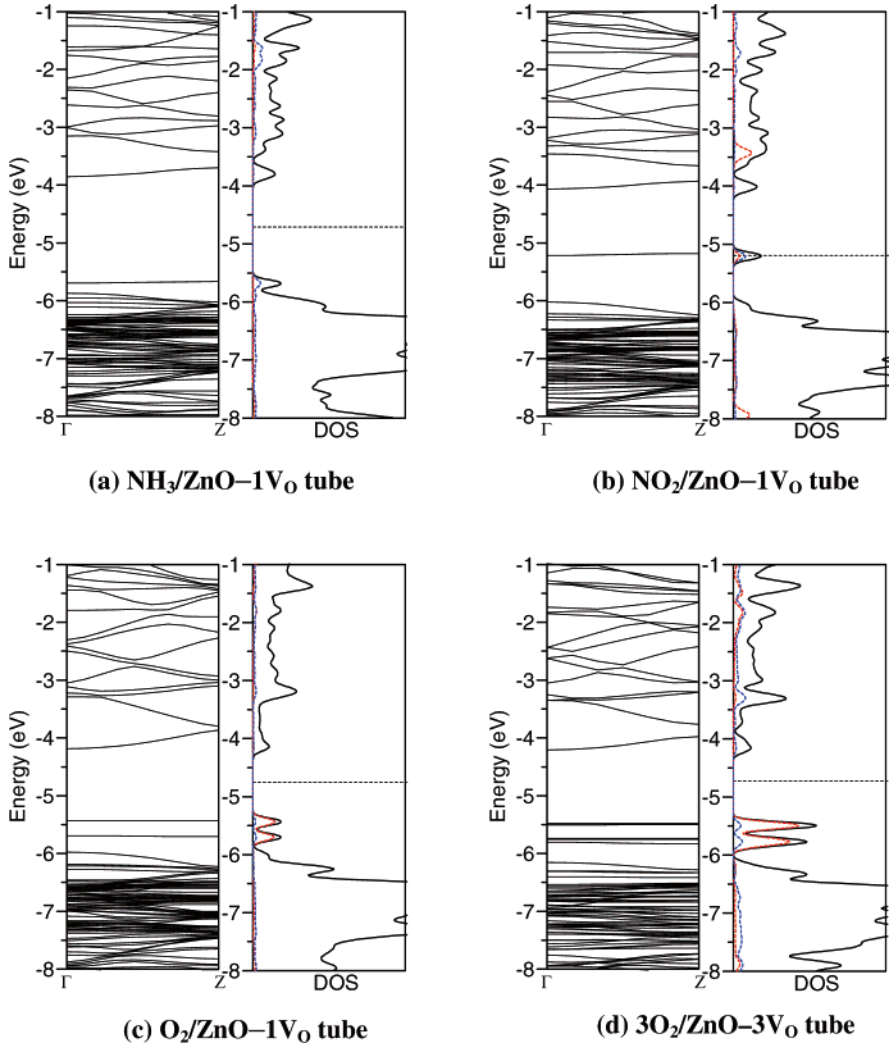

Figure 7. Electronic band structures and total DOS for various adsorbate on the ZnO (6,0)−V_O SWNT (Figure 4). Local DOS projected onto adsorbates and Zn atoms near the V_O site are plotted on red and blue dashed lines, respectively.

mechanism in that when depletion layers are formed on the surface of *n*-type semiconductor after sufficient exposure to oxygen the concentration of major carrier (electron) will be reduced and so is the electrical conductance of the sensor.

The adsorption energy of NO_2 on the V_O site is also increased significantly to $E_{ad} = -0.98$ eV, three times larger than $E_{ad} = -0.30$ eV on the perfect site. Furthermore, the adsorbed NO_2 can dissociate into one adsorbed O atom and NO molecule with an activation barrier of 0.49 eV as shown in Figure 5 and Table 2. This dissociation process is exothermic and is likely to occur at room temperature. Like O_2, the dissociated O atom from NO_2 will fill the V_O site while the remaining NO molecule can desorb easily via an exothermic process ($E_{ad} = 0.042$ eV) on a defect-free surface.

The binding energy of NH_3 on the V_O site is increased slightly to $E_{ad} = -0.91$ eV from $E_{ad} = -0.82$ eV on the perfect site, with nearly the same charge transfer $\delta q = 0.25e$, suggesting that the adsorption of NH_3 is weakly affected by the V_O defect.

To investigate the effect of adsorbate coverage on the adsorption energy, we also calculated the adsorption of NO_2 and NH_3 on the ZnO (6,0) SWNT with $^1/_6$ and $^1/_3$ monolayer (ML) coverage. Only highly symmetric coverage is considered here. It is found that the average adsorption energy is reduced with increasing the coverage of adsorbates, concomitant with the increase in d and the decrease in δq (Table 1).

In summary, the sensitivity of ZnO (6,0) SWNT as a gas-molecule sensor is expected to be enhanced with increasing concentration of the V_O sites due to stronger interactions between target molecules and the V_O sites. But the sensitivity can be reduced dramatically after exposure to O_2 or NO_2 because of the remediation of the V_O defects via the dissociation of O_2 or NO_2. In air, it is difficult to prevent the gas sensor from exposure to O_2. Therefore, the target molecules must compete with O_2 for the surface adsorption or possibly react with the adsorbed atomic O species. This latter scenario is, however, beyond the scope of this study.

3.3. Electronic Structure of the ZnO (6,0) SWNT upon Molecule Adsorption. The tuning effect of adsorbed molecules on the electrical conductance of ZnO nanotube underlies the working mechanism of gas sensors for detecting the target molecules. To gain more insight into the adsorbate/nanotube interaction, we calculated the electronic structure of the combined adsorbate/ZnO (6,0) SWNT system where the adsorbates are in their optimal configurations as shown in Figures 2−4. As mentioned in Section 3.1, although the DFT-PBE method underestimates the band gap it still yields reasonably correct features of electronic structure. Here, we only consider the position of impurity states and the change of Fermi level upon molecule adsorption. The calculated band structure and total density of states (DOS) as well as local DOS projected onto adsorbates are plotted in Figures 6 and 7. It can be seen

that the adsorption of a single H_2, CO, and NH_3 molecule per supercell does not introduce any impurity states within the band gap of the pristine ZnO (6,0) SWNT. The CO molecule does introduce some impurity states within the conduction band (CB), ~2 eV above the Fermi level. In contrast, the O_2 and NO_2 molecules can give rise to some impurity states within the band gap of the pristine ZnO (6,0) SWNT, thereby modifying the electronic structures of the ZnO tube. The O_2 molecule induces impurity states that overlap with the Fermi level (Figure 6c). The NO_2 molecule introduces occupied and unoccupied impurity states, where the unoccupied states locate near the CB edge (Figure 6g).

When the coverage of NH_3 is increased, the NH_3 molecules can lift the Fermi level of the system substantially, which leaves fewer states near the CB edge, but the band gap remains unchanged (Figure 6e and f). For NO_2, the increase of coverage leads to two major changes in the band structures: (1) much more impurity states near the band edge, and (2) the Fermi level is pushed downward (Figure 6h and i), suggesting that the ZnO (6,0) SWNT would be a good sensor to NO_2 gas. Note that the electronic structures for ZnO (6,0) SWNT with $^1/_6$ and $^1/_3$ ML coverage of NH_3 and NO_2 were calculated based on one periodicity of adsorbate/ZnO (6,0) NT, that is, one-third of the original supercell size. Accordingly, the density of states shown in Figure 6e, f, h, and i appeared somewhat smaller.

On the ZnO nanotube containing one V_O site, the adsorption of a single NH_3 molecule does lead to some impurity states near the VB edge (Figure 7a). For NO_2, a localized impurity band is formed in the middle of band gap, overlapping with the Fermi level (Figure 7b). For O_2, because of the dissociative adsorption on the defected ZnO nanotube, the number of impurity states increases significantly as the coverage of O_2 and V_O defects is increased, thereby reducing the band gap. These impurity states are mainly contributed by the dissociated O_2 (Figure 7c and d).

4. Conclusions

We have studied the structural and electronic properties of a prototype ZnO (6,0) SWNT. The pristine nanotube is semiconducting with a direct band gap larger than that of the bulk ZnO. The valence and conduction bands are contributed mainly by the p orbitals of O and s orbitals of Zn atoms, respectively. When the nanotube contains V_O defects, localized states are induced above the valence band and below the conduction band.

We have also investigated the adsorption of H_2, CO, NH_3, O_2, and NO_2 on the ZnO (6,0) SWNT. (1) Adsorbate CO or NH_3 can lead to partial charge transfer to the ZnO nanotube, whereas adsorbate O_2 and NO_2 can lead to partial charge transfer from the ZnO nanotube, consistent with experimental observations on the charge-transfer behavior of *n*-type ZnO NR sensors when exposed to these gas molecules. (2) O_2 and H_2 are physisorbed on the sidewall of defect-free ZnO (6,0) SWNT, while CO, NH_3, and NO_2 are molecularly chemisorbed. (3) O_2 and NO_2 undergo a dissociative chemisorption at the V_O site via filling the V_O with one O atom originated from the adsorbate. The dissociation of O_2 is exothermic and barrierless while the dissociation of NO_2 is also exothermic but entails a small activation barrier (0.49 eV). (4) The electron-donor molecules (CO and NH_3) tend to enhance the concentration of major carriers (electrons), whereas the electron-acceptor molecules (O_2 and NO_2) tend to reduce the concentration. Finally, the calculated electronic structures of the combined ZnO (6,0) SWNT/adsorbate systems provide additional insight into the gas/ZnO nanotube interaction and thereby gas-specific information about the ZnO SWNT as a sensor.

Acknowledgment. This research was supported in part by grants from DOE (DE-FG02-04ER46164), NSF (CHEM and CMMI), and the Nebraska Research Initiative, and by the Research Computing Facility at University of Nebraska-Lincoln.

Supporting Information Available: Band structures of bulk ZnO and ZnO (6,0) SWNT without and with one V_O defect site calculated using DFT-B3LYP method implemented in the CRYSTAL06 package. This material is available free of charge via the Internet at http://pubs.acs.org.

References and Notes

(1) (a) Yamazoe, N. *Sens. Actuators, B* **1991**, *5*, 7. (b) Sberveglieri, G. *Sens. Actuators, B* **1995**, *23*, 103.

(2) (a) Schmidt-Mende, L.; MacManus-Driscoll, J. L. *Mater. Today* **2007**, *10*, 40. (b) Özgür, Ü.; Alivov, Ya. I.; Liu, C.; Teke, A.; Reshchikov, M. A.; Doğan, S.; Avrutin, V.; Cho, S.-J.; Morkoç, H. *Appl. Phys. Rev.* **2005**, *98*, 041301.

(3) Trivikrama Rao, G. S.; Tarakarama Rao, D. *Sens. Actuators, B* **1999**, *55*, 166.

(4) Yamazaki, T.; Wada, S.; Noma, T.; Suzuki, T. *Sens. Actuators, B* **1993**, *14*, 594.

(5) Chatterjee, A. P.; Mitra, P.; Mukhopadhyay, A. K. *J. Mater. Sci.* **1999**, *34*, 4225.

(6) (a) Nenov, T.; Yordanov, S. *Sens. Actuators, B* **1992**, *8*, 117. (b) Rao, B. B. *Mater. Chem. Phys.* **2000**, *64*, 62.

(7) Xu, J.; Pan, Q.; Shun, Y.; Tian, and Z. *Sens. Actuators, B* **2000**, *66*, 277.

(8) Lin, H.; Tzeng, S.; Hsiau, P.; Tsai, W. *Nanostruct. Mater.* **1998**, *10*, 465.

(9) Baratto, C.; Sberveglieri, G.; Onischuk, A.; Caruso, B.; di Stasio, S. *Sens. Actuators, B* **2004**, *100*, 261.

(10) Li, Q. H.; Liang, Y. X.; Wan, Q.; Wang, T. H. *Appl. Phys. Lett.* **2004**, *85*, 6389.

(11) Fan, Z.; Wang, D.; Chang, P. C.; Tseng, W. Y.; Lu, J. G. *Appl. Phys. Lett.* **2004**, *85*, 5923.

(12) (a) Wang, H. T.; Kang, B. S.; Ren, F.; Tien, L. C.; Sadik, P. W.; Norton, D. P.; Pearton, S. J.; Lin, J. *Appl. Phys. Lett.* **2005**, *86*, 243503. (b) Kang, B. S.; Heo, Y. W.; Tien, L. C.; Norton, D. P.; Ren, F.; Gila, B. P.; Pearton, S. J. *Appl. Phys. A* **2005**, *80*, 1029.

(13) (a) Rout, C. S.; Kulkarni, G. U.; Rao, C. N. R. *J. Phys. D: Appl. Phys.* **2007**, *40*, 2777. (b) Xu, J. Q.; Chen, Y. P.; Chen, D. Y.; Shen, J. N. *Sens. Actuators, B* **2006**, *113*, 526. (c) Xu, J. Q.; Chen, Y. P.; Li, Y. D.; Shen, J. N. *J. Mater. Sci.* **2005**, *40*, 2919.

(14) Wang, J. X.; Sun, X. W.; Yang, Y.; Huang, H.; Lee, Y. C.; Tan, O. K.; Vayssieres, L. *Nanotechnology* **2006**, *17*, 4995.

(15) Fan, Z.; Lu, J. G. *Appl. Phys. Lett.* **2005**, *86*, 123510.

(16) Wang, X.; Zhang, J.; Zhu, Z. *Appl. Surf. Sci.* **2006**, *252*, 2404.

(17) Liao, L.; Lu, H. B.; Li, J. C.; He, H.; Wang, D. F.; Fu, D. J.; Liu, C.; Zhang, W. F. *J. Phys. Chem. C* **2007**, *111*, 1900.

(18) Wang, C. H.; Chu, X. F.; Wu, M. M. *Sens. Actuators, B* **2006**, *113*, 320.

(19) Wan, Q.; Li, Q. H.; Chen, Y. J.; Wang, T. H.; He, X. L.; Li, J. P.; Lin, C. L. *Appl. Phys. Lett.* **2004**, *84*, 3654.

(20) Wei, A.; Sun, X. W.; Wang, J. X.; Lei, Y.; Cai, X. P.; Li, C. M.; Dong, Z. L.; Huang, W. *Appl. Phys. Lett.* **2006**, *89*, 123902.

(21) Wu, J. J.; Liu, S. C.; Wu, C. T.; Chen, K. H.; Chen, L. C. *Appl. Phys. Lett.* **2002**, *81*, 1312.

(22) Kong, X. H.; Sun, X. M.; Li, X. L.; Li, Y. D. *Mater. Chem. Phys.* **2003**, *82*, 997.

(23) Kong, X. Y.; Ding, Y.; Wang, Z. L. *J. Phys. Chem. B* **2004**, *108*, 570.

(24) (a) Sun, Y.; Riley, D. J.; Ashfold, M. N. R. *J. Phys. Chem. B* **2006**, *110*, 15186. (b) Xu, W. Z.; Ye, Z. Z.; Ma, D. W.; Lu, H. M.; Zhu, L. P.; Zhao, B. H.; Yang, X. D.; Xu, Z. Y. *Appl. Phys. Lett.* **2005**, *87*, 093110.

(25) (a) Wang, P. M.; Xing, Y. J.; Xu, J.; Yu, D. P. *New J. Phys.* **2003**, *5*, 115. (b) Zhang, X.; Zhang, Y.; Xu, J.; Wang, Z.; Chen, X.; Yu, D.; Zhang, P.; Qi, H.; Tian, Y. *Appl. Phys. Lett.* **2005**, *87*, 123111.

(26) Lin, C.-C.; Chen, H.-P.; Chen, S.-Y. *Chem. Phys. Lett.* **2005**, *404*, 30.

(27) Jiang, Z.-Y.; Xu, T.; Xie, Z.-X.; Lin, Z.-W.; Zhou, X.; Xu, X.; Huang, R.-B.; Zheng, L.-S. *J. Phys. Chem. B* **2005**, *109*, 23269.

(28) Erkoc, S.; Kökten, H. *Physica E* **2005**, *28*, 162.

(29) Tu, Z. C.; Hu, X. *Phys. Rev. B* **2006**, *74*, 035434.

(30) (a) Shen, X.; Allen, P. B.; Muckerman, J. T.; Davenport, J. W.; Zheng, J.-C. *Nano Lett.* **2007**, *7*, 2267. (b) Elizondo, S. L.; Mintmire, J. W. *J. Phys. Chem. C* **2007**, *113*, 7756.

(31) (a) Delley, B. *J. Chem. Phys.* **1990**, *92*, 508. (b) Delley, B. *J. Chem. Phys.* **2003**, *113*, 7756. (c) DMol^3 is available from Accelrys.

(32) Perdew, J. P.; Burke, K.; Ernzerhof, M. *Phys. Rev. Lett.* **1996**, *77*, 3865.
(33) Monkhorst, H. J.; Pack, J. D. *Phys. Rev. B* **1976**, *13*, 5188.
(34) (a) Henkelman, G.; Jonsson, H. *J. Chem. Phys.* **2000**, *113*, 9978. (b) Olsen, R. A.; Kroes, G. J.; Henkelman, G.; Arnaldsson, A.; Jonsson, H. *J. Chem. Phys.* **2004**, *121*, 9776.
(35) An, W.; Wu, X.; Yang, J. L.; Zeng, X. C. *J. Phys. Chem. C* **2007**, *111*, 14105.
(36) Zhang, S. B.; Wei, S.-H.; Zunger, A. *Phys. Rev. B* **2001**, *63*, 075205.
(37) Zhou, G. C.; Sun, L. Z.; Zhong, X. L.; Chen, X. S.; Wei, L.; Wang, J. B. *Phys. Lett. A* **2007**, *368*, 112.
(38) Kan, E.-J.; Yuan, L.-F.; Yang, J. *J. Appl. Phys.* **2007**, *102*, 033915.
(39) Dovesi, R. R. et al. *CRYSTAL 2006* User's Manual; University of Torino: Torino, 2006.
(40) Wöll, C. *Prog. Surf. Sci.* **2007**, *82*, 55.
(41) Yan, Y.; Al-Jassim, M.M.; Wei, S.-H. *Phys. Rev. B* **2005**, *72*, 161307(R).